Reconfigurable 3D photonic lattices by optical induction for optical control of beam propagation

Article *in* Applied Physics B · July 2011

DOI: 10.1007/s00340-011-4659-0

Appl Phys B (2011) 104:553–560
DOI 10.1007/s00340-011-4659-0

Applied Physics B
Lasers and Optics

INVITED PAPER

Reconfigurable 3D photonic lattices by optical induction for optical control of beam propagation

P. Zhang · N.K. Efremidis · A. Miller · P. Ni · Z. Chen

Received: 26 April 2011 / Revised version: 23 May 2011 / Published online: 30 July 2011

Abstract We report on our recent theoretical and experimental studies of three-dimensional (3D) photonic lattice structures which are established in a bulk nonlinear crystal by employing different optical induction techniques. These 3D photonic lattices bring about new opportunities for controlling the flow of light via coupling engineering originated from the lattice modulation along the beam propagation direction. By fine tuning the lattice parameters, we observe a host of unusual behaviors of beam propagation in such reconfigurable 3D lattices, including enhanced discrete diffraction, light tunneling inhibition—better known as coherent destruction of tunneling (CDT), anomalous diffraction, negative refraction, as well as CDT-based image transmission. In addition, we propose and demonstrate a new way of creating 3D ionic-type photonic lattices by controlled Talbot effect.

1 Introduction

Photonic band gap materials and optical periodic structures in general have been studied for decades due to their capabilities of controlling the flow of light [1]. The 'holy grail' of photonic structures is to manipulate light with periodic index modulation in all three dimensions. However, it has been a great challenge to create three-dimensional (3D) structures in bulk media at microscopic length scale. Thus far, various techniques have been proposed and developed for fabricating 3D photonic structures, from mechanical hole drilling to semiconductor microfabrication, from self-assembly and colloidal crystallization to advanced layer-by-layer fabrication, and from laser-induced deposition to holographic lithography [2–8]. Instead of manipulating wave propagation in time-domain frequency with photonic crystals fabricated for microwaves and visible light, closely spaced waveguide arrays (photonic lattices) have been identified as ideal band gap materials for controlling light dynamics in the spatial-frequency domain [9–12]. A convenient way for creating reconfigurable photonic lattices is to use 'optical induction' in nonlinear crystals [13]. Thus far, optically induced one- or two-dimensional (1D or 2D) photonic lattices have served as a platform for investigating a variety of fascinating linear and nonlinear wave phenomena, especially for the demonstrations of spatial discrete or gap solitons [14–17]. However, experimental study of beam dynamics in 3D photonic lattices has been hampered due to the difficulties in fabricating or inducing desired 3D lattice structures. Even in 1D and 2D domains, lattice reconfiguration or modulation along the longitudinal propagation direction can lead to many intriguing discrete wave phenomena (e.g. diffraction and refraction management, inhibition of light tunneling, multi-color dynamic localization, Rabi oscillation and negative coupling [18–31]). Therefore, it is expected that much richer phenomena could occur in 3D photonic lattices. For instance, it has been proposed that 3D photonic structures can be used for image transmission [32] and for studying 3D vortex structures [33].

P. Zhang · A. Miller · P. Ni · Z. Chen (✉)
Department of Physics and Astronomy, San Francisco State University, San Francisco 94132, USA
e-mail: zhigang@sfsu.edu

N.K. Efremidis
Department of Applied Mathematics, University of Crete, Heraklion, Crete 71409, Greece

Z. Chen
The Key Laboratory of Weak-Light Nonlinear Photonics, Ministry of Education and TEDA Applied Physics School, Nankai University, Tianjin 300457, China

Recently, 3D photonic lattices have been successfully created with the optical induction technique [34–38], and some unusual beam dynamics in these 3D lattices have been observed [34, 35].

In this paper, we provide a brief overview of our recent work on controlling beam propagation with optically induced 3D photonic lattices. We show that various 3D photonic lattice structures can be established in a bulk nonlinear crystal by employing different optical induction techniques, including the superposition of a pair of 2D photonic lattices along different directions and precise control of the Talbot effect. By fine tuning the lattice parameters such as lattice modulation and spacing, we demonstrate unusual behaviors of beam propagation in these reconfigurable 3D photonic lattices, including enhanced discrete diffraction, light tunneling inhibition or coherent destruction of tunneling (CDT), anomalous diffraction, as well as negative refraction. In addition, CDT-mediated image transmission in 3D photonic lattices is proposed and an example is demonstrated as a proof of principle. We also discuss the possibility of formation of 3D ionic-type photonic lattices by controlled Talbot effect for beam manipulation.

2 Enhanced diffraction in scaffold and fishnet photonic lattices

Firstly, we optically induce 3D photonic lattices in a bulk nonlinear crystal by overlapping a pair of 2D square lattices and monitor the linear discrete diffraction of a probe beam through the induced lattices. Our method is depicted in Fig. 1a, where two 2D grid-like lattice-inducing beams are launched into the crystal from two orthogonal directions (both perpendicular to the crystalline c-axis) and are superimposed to form 3D lattice structures inside the crystal. Simply by switching the polarity of the bias field, a scaffold- or fishnet-type 3D lattice structure (Figs. 1b and 1c) is generated under a self-focusing or self-defocusing photorefractive screening nonlinearity [13–17]. Our experimental setup with a biased photorefractive SBN:60 crystal (strontium barium niobate, dimension: $a \times a \times c = 5\ \text{mm} \times 10\ \text{mm} \times 5\ \text{mm}$) is shown in Fig. 1d. Two sets of square lattices are induced by sending ordinarily polarized partially coherent light beams (diffused light from an argon ion laser operating at 488 nm) through amplitude masks, as used in our earlier work [16, 17]. The two lattice-inducing beams spatially modulated by the masks are sent through the crystal from two orthogo-

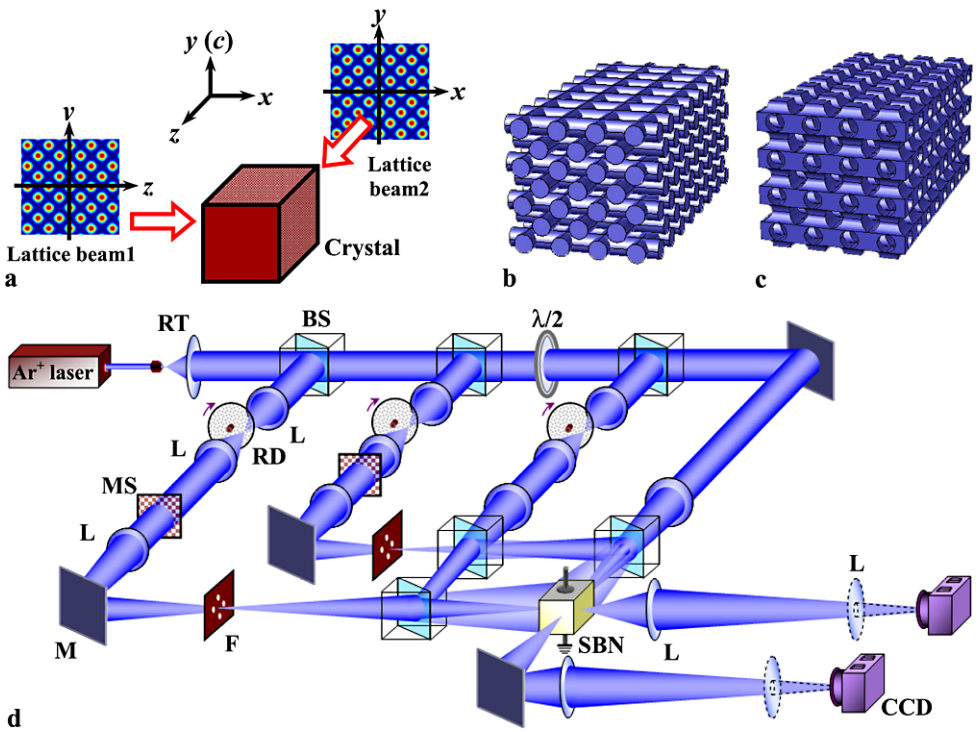

Fig. 1 (**a**) Schematic drawing of the optical induction method for scaffold and fishnet photonic lattices. The crystalline c-axis of the nonlinear crystal is oriented along the y-direction. The two lattice-inducing beams are launched along two crystalline a-axes (oriented along x- and z-directions). (**b**, **c**) Illustration of induced scaffold and fishnet lattice structures under self-focusing and self-defocusing nonlinearity, respectively. (**d**) Experimental setup for inducing and monitoring 3D photonic lattices in a biased SBN crystal. The left two beam paths are for two lattice-inducing beams, the third path is for Brillouin zone spectrum measurement, and the fourth (*far right*) path is for testing the diffraction of a focused probe beam. *RT*: reversed telescope; *BS*: beam splitter; *RD*: rotating diffuser; *L*: lens; *MS*: amplitude mask; *M*: mirror; *F*: Fourier-plane filter; $\lambda/2$: half-wave plate

nal directions. By employing a proper spatial filter at the Fourier plane of each mask, the Talbot self-imaging can be totally suppressed, so that the transversely periodic light pattern remains invariant during the propagation throughout the crystal [16, 17, 39–41]. A dc field is applied along the y-direction (corresponding to the crystalline c-axis, which is oriented perpendicular to the propagation directions of all beams in the crystal). With the bias field, the periodic intensity patterns induce periodic index changes in the otherwise uniform crystal, resulting in 3D photonic lattice structures. To probe the induced lattice structures, a broad beam (close to a uniform plane wave) is sent through the lattice to obtain a near-field pattern of plane-wave guidance. Another partially coherent beam (generated by a third rotating diffuser) is focused and split into two parts to obtain the Brillouin zone (BZ) spectrum from two orthogonal directions using the method as depicted in [42, 43]. In addition, a coherent beam from the same laser (not passed through a diffuser) is used as a probe beam to test the discrete diffraction properties of the induced 3D lattices. Note that, when inducing the lattice structures, ordinarily polarized light beams are used, but for probing the induced lattices (including plane-wave guidance, BZ spectrum, and discrete diffraction), extraordinarily polarized probe beams are used [16, 17]. The near-field and far-field patterns of the lattice beams and the spatial Fourier spectrum of the probe beam are monitored with imaging lenses and CCD cameras. For all experiments, the crystal is illuminated when necessary with an incoherent background beam from a white light source to fine tune the nonlinearity [14–17].

Typical experimental results of optically induced 3D photonic lattices are shown in Fig. 2. The two 2D lattice-inducing beams with the same periodicity (20 μm) and intensity are fine tuned to overlap from two orthogonal directions to generate the 3D periodic intensity pattern in the SBN crystal. With a bias field of 1.8 kV/cm applied appropriately along the crystalline c-axis, the crystal turns into a *self-focusing* medium. The induced lattice structures monitored under this condition are shown in Figs. 2a and 2b, where the near-field patterns from plane-wave guidance (a) along with the BZ spectra (b) of the index lattices from the two orthogonal directions are displayed. It can be seen that due to the lattice superposition, the near-field pattern possesses 2D periodic modulation in both orthogonal directions, as shown in Fig. 2a. The 2D square-like lattice structures are further visualized by the BZ spectrum (Fig. 2b). It is evident that the 2D index lattices are established in two orthogonal directions, thus forming effectively a 3D lattice in the bulk nonlinear crystal.

Next, solely by reversing the polarity of the bias field (i.e. changing it to −1.8 kV/cm), 3D photonic lattices under *self-defocusing* nonlinearity are also established. Figures 2c and 2d depict our experimental results, where (c) and (d)

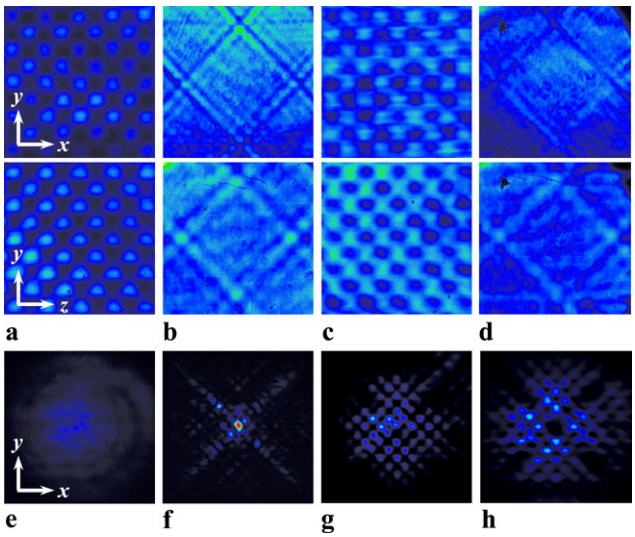

Fig. 2 Experimental results for optically induced scaffold (**a**, **b**, **e**–**h**) and fishnet (**c**, **d**) 3D lattices. (**a**, **c**) Plane-wave guidance in induced 3D lattices; (**b**, **d**) Brillouin zone spectra of (**a**, **c**), where the upper and lower rows correspond to results obtained after 10 mm and 5 mm propagation inside the crystal. (**e**–**h**) Diffraction enhancement in a 3D scaffold photonic lattice, where (**e**) is the output of a probe beam propagating along the z-direction without lattice and (**f**–**h**) its output discrete diffraction patterns after propagating through the lattice when the intensity of the lattice-inducing beam along the x-direction (see Fig. 1) is gradually increased

correspond to lattice near-field patterns and BZ spectra obtained from two orthogonal directions, respectively. From the near-field patterns of Fig. 2c, it is clear that the induced index lattices possess a 'backbone' or "fishnet" structure, quite different from those of Figs. 2a and 2b obtained under the self-focusing nonlinearity, although the BZ spectra are somewhat similar. We expect that waveguide coupling, band gap structure, and beam dynamics in such lattices should be quite different from those in self-focusing lattices. In addition, it is apparent that the index modulation (contrast) of the lattices is lower than that created under the self-focusing nonlinearity. Indeed, under a negative bias field, the SBN crystal is susceptible to depolarization, so it is a challenge to achieve a high index contrast for opening the higher band gaps in the 'backbone' photonic lattices [44].

Finally, we present experimental results on discrete diffraction of a probe beam propagating along the z-direction through the 3D lattice induced under self-focusing nonlinearity. To assure linear propagation of the probe beam, its intensity is adjusted to be very low and its output patterns are taken nearly instantaneously once the beam is launched. Typical experimental results are summarized in Figs. 2e–2h. For these results, the period of the two lattice beams is about 40 μm, the intensity of lattice beam 2 (see Fig. 1a) is fixed, but the intensity of lattice beam 1 is varied. Three examples of discrete diffraction patterns in the x–y output plane from the crystal are shown in Figs. 2f–2h, where the

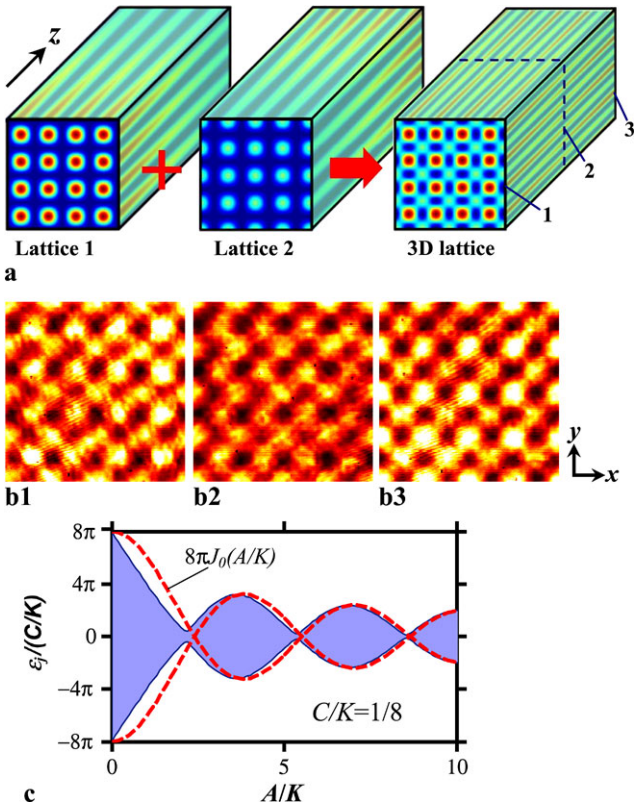

Fig. 3 (**a**) Schematic of optical induction of 3D lattices in a biased nonlinear crystal by superposition of two lattice beams with opposite intensity gradient along z; (**b**) experimental results of transverse patterns taken at three different z-positions marked in *right-hand panel* of (**a**), corresponding to input, *middle*, and output facets of the crystal; (**c**) numerical (*shaded areas*) and analytical (*dashed curve*) results of Floquet quasi-energies ε_j vs. lattice modulation for the induced 3D photonic lattices

intensity ratio between lattice beam 2 and lattice beam 1 is varied from 1:0, to 1:1, and to 1:2. Thus, discrete diffraction is enhanced dramatically in 3D lattices (Figs. 2g and 2h) as compared to that in the 2D lattices (Fig. 2f), and it is apparent that the enhancement increases as the lattice modulation gets stronger in the propagation direction. Intuitively, we can understand that such diffraction enhancement results from increased coupling among waveguides oriented along the z-direction when they are joining by waveguides oriented along the transverse direction. Indeed, these experimental results are also corroborated with our numerical simulations [34].

3 Coherent destructive tunneling in out-of-phase z-modulated lattices

It has been shown that light inhibition due to CDT can occur in photonic lattices with out-of-phase index modulations along the longitudinal direction [23–25]. To construct such lattice structures in three dimensions, we propose an optical induction method as shown in Fig. 3a, where the 3D lattice-inducing beams are composed by superposition of two mutually incoherent lattice beams with opposite intensity gradient along the z-direction (note that each lattice beam has in-phase z-modulation, and only a half of a z-period is shown here). In our experiment, due to the need to match the waveguide coupling length and the limitation of our crystal length (2-cm-long SBN:60 crystal), we generate a 3D lattice (30 μm transverse lattice spacing) with only a half modulation period along the z-direction by overlapping two mutually incoherent lattice beams—one has decreasing intensity from input to output facets of the crystal while the other has increasing intensity, yet it is enough for observing the predicated phenomena in the 3D photonic lattices as a proof of principle [35]. By adjusting the imaging plane of the amplitude mask and the spatial coherence of the lattice-inducing beams, the intensity gradient along the z-direction for each lattice beam is changed individually. Therefore, the induced structure can be 'fine tuned' by varying the intensity gradients of the two lattice-inducing beams while keeping the total beam intensity in the middle of the crystal essentially unchanged. Figure 3b shows a few typical snapshots of the lattice pattern taken at different transverse planes of the crystal.

To analyze the beam dynamics in our optically induced 3D lattice, let us start with a coupled-mode theory model

$$i\frac{\mathrm{d}u_{m,n}}{\mathrm{d}z} + C(u_{m+1,n} + u_{m-1,n} + u_{m,n+1} + u_{m,n-1}) + \frac{A}{2}(-1)^{m+n}\cos(Kz)u_{m,n} = 0 \quad (1)$$

where C is the coupling coefficient between adjacent waveguides, $A/2$ is the amplitude, and K determines the spatial frequency of the propagation constant modulation along z. Note that the propagation constant modulation is out-of-phase between nearest neighbors. Using the asymptotic analysis, we obtain the effective (or average) coupling coefficient as $\bar{C} = CJ_0(A/K)$. Thus, asymptotically the optical field will satisfy

$$i\frac{\mathrm{d}v_{m,n}}{\mathrm{d}z} + \bar{C}(v_{m+1,n} + v_{m-1,n} + v_{m,n+1} + v_{m,n-1}) = 0, \quad (2)$$

where

$$u_{m,n} = v_{m,n}\exp\left[i\frac{(-1)^{m+n}A}{2K}\sin(Kz)\right]. \quad (3)$$

In addition, by numerically employing the Floquet theory [45], the coefficient $\bar{C}$ is computed from the quasi-energy band edges. In particular, (1) can be expressed in vector form as

$$i\frac{\mathrm{d}U}{\mathrm{d}z} + A(z)U = 0, \quad (4)$$

where $U = [u_{1,1}, u_{1,2}, \ldots, u_{N,N}]^{\mathrm{T}}$ and $A(z)$ is the corresponding matrix. We formally integrate (4) to obtain

$$U(z) = \exp\left(-i\int_0^z A(s)\mathrm{d}s\right)U(0) = F(z)U(0), \tag{5}$$

where z ordering should be applied to evaluate the above operator. We define the Floquet operator as $B = F(2\pi/K)$, where $2\pi/K$ is the period of the oscillations along z. Then, according to the Floquet theorem, the eigenvectors and eigenvalues of the Floquet operator are given by

$$BU_j = \exp(-i\varepsilon_j)U_j, \tag{6}$$

where $\varepsilon_j$are referred to as the Floquet quasi-energies. The quasi-energies form a band, and the band edges can be associated to the effective coupling coefficient via the relation $|\bar{C}| = K\max(\varepsilon_j)/8\pi$. As a result, the theoretical prediction for the quasi-energy band edges is given by $\max(\varepsilon_j) = 8\pi(C/K)|J_0(2A/K)|$. Figure 3c depicts typical numerical (solid curve) and analytical (dashed curve) results, which show that the coupling coefficient oscillates between positive and negative values as the modulation parameter A/K along the z-direction varies. In particular, the coefficient $\bar{C}$ approaches zero at certain points, which corresponds to the CDT condition under which inhibition of light tunneling occurs. Near these zero-coupling points, discrete diffraction of light due to waveguide coupling is dramatically suppressed, providing a new way for distortion-free image transmission. Furthermore, $\bar{C}$ can become negative at some increased modulations, leading to possible reversal of band gap structures [46, 47]. It is in these negative-coupling regimes that one expects to see anomalous diffraction and negative refraction associated with band reversal within the first Brillouin zone [46–49].

Our experimental demonstration of the aforementioned phenomenon is summarized in Fig. 4. By sending a circular Gaussian beam (Fig. 4a1) into the 3D lattice established in Fig. 3b, the property of discrete diffraction in the 3D photonic lattice at different z-modulations is examined. As expected from the theory, without z-modulation (corresponding to a 2D lattice), the probe beam exhibits strong discrete diffraction (Fig. 4a2), but such diffraction is completely suppressed at a certain increased z-modulation corresponding to the CDT condition (Fig. 4a3). However, coupling-induced diffraction comes back with further increase of the z-modulation (Fig. 4a4). In fact, as the modulation is increased even further, we found that higher-order CDT also takes place due to the oscillation of the coupling coefficient as shown in Fig. 3c. Under similar conditions, we demonstrate the principle of image transmission at the CDT condition. To do so, we simply launch an input image of a '+' pattern (Fig. 4b1) into the lattice structure and examine the output at different levels of z-modulation. In the 2D lattice, the input image is strongly distorted after propagating through the lattice (Fig. 4b2). However, in the 3D photonic lattice under the CDT condition, the input image maintains its shape after linear propagation without severe distortion (Fig. 4b3). As expected, further increase of z-modulation leads to image distortion again (Fig. 4b4). Next, we demonstrate anomalous diffraction and negative refraction in the negative-coupling regime. According to our theory, the index modulation of the 3D lattice corresponding to Figs. 4a4 and 4b4 leads to a negative effective coupling coefficient. Results for the diffraction/refraction management under this condition are displayed in Figs. 4c and 4d. To visualize the anomalous diffraction under the linear condition, a focused Gaussian beam is launched and monitored while propagating through the crystal (Fig. 4c). For the experiment of negative refraction, the Gaussian beam is tilted toward the left at the half

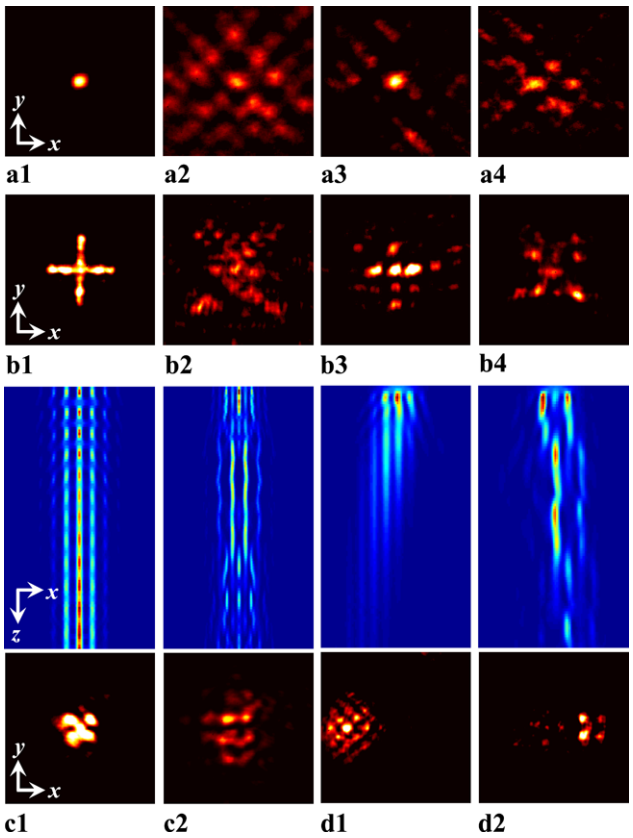

Fig. 4 Experimental demonstrations of coherent destructive tunneling of a focused Gaussian probe beam (**a**) and image transmission of a '+' shape (**b**), where *(1)* depicts the input and *(2–4)* show output transverse patterns at gradually increased index modulations along the z-direction. (**c**) and (**d**) show numerical (*upper panels*) and experimental (*bottom panels*) results of beam diffraction (**c**) and refraction (**d**) in 2D (*left*, c1 and d1) and 3D (*right*, c2 and d2) lattices. For diffraction (**c**), the Gaussian probe beam is launched straight along the z-direction but initially focused at the crystal output. For refraction (**d**), the beam is initially toward left relative to the z-direction. The *upper panels* show side views of a probe beam propagating inside the lattices, while the bottom ones show output transverse patterns

of the 1st-order Bragg angle of the 2D lattice (without z-modulation) (Fig. 4d). Obviously, in the 2D lattice, the beam undergoes normal diffraction and refraction, as it does in a homogeneous medium (Figs. 4c1 and 4d1). However, when the effective coupling coefficient is negative, the initially focused Gaussian beam diverges (Fig. 4c2), and the initially left-tilted beam bends toward the right (Fig. 4d2), exhibiting typical behavior of anomalous diffraction and negative refraction [35]. These experimental observations agree well with our theoretical results. Note that the negative refraction observed here does not require the two-beam excitation scheme as used in previous experiments [30, 48], reflecting a rather different mechanism.

4 Three-dimensional ionic-type photonic lattices by controlled Talbot effect

Our previous work demonstrated that active control of the Talbot effect of a broad beam as periodically modulated by an amplitude optical mask provides an effective tool for generating various 2D photonic lattices (including ionic-type photonic lattices) in bulk nonlinear crystals [16, 17, 39–41, 49, 50]. Here, we show that reconfigurable 3D photonic lattices can be optically induced as well by tailoring the Talbot effect. As a matter of fact, the Talbot effect can be explained by multi-beam interference. Therefore, to understand the principle of our method, we first analyze the optical field generated by five-beam interference (such as by selecting the 0th- and the four 1st-order diffraction patterns from a typical square lattice) as follows:

$$\begin{aligned} U(x,y,z) = {} & A_0 \exp(ikz) \\ & + A_1 \exp\left[ik(x+y)\cos\alpha + ikz\cos\gamma\right] \\ & + A_1 \exp[-ik(x+y)\cos\alpha + ikz\cos\gamma] \\ & + A_1 \exp\left[ik(x-y)\cos\alpha + ikz\cos\gamma\right] \\ & + A_1 \exp\left[-ik(x-y)\cos\alpha + ikz\cos\gamma\right], \end{aligned} \quad (7)$$

where A_0 and A_1 determine the amplitudes of the 0th- and 1st-order diffracted light, k is the wave number, and α and γ denote the angles between the beams and the principal coordinate axes. Then the intensity distribution of the lattice beam $I(x,y,z)$ can be expressed as

$$\begin{aligned} I(x,y,z) = {} & |A_0|^2 + 16|A_1|^2 \cos^2(kx\cos\alpha)\cos^2(ky\cos\alpha) \\ & + 8A_0A_1\cos\left[kz(1-\cos\gamma)\right] \\ & \times \cos(kx\cos\alpha)\cos(ky\cos\alpha). \end{aligned} \quad (8)$$

Apparently, the first term is a uniform background, the second one represents a square lattice without z-modulation, and the last one represents a 3D ionic-type photonic lattice

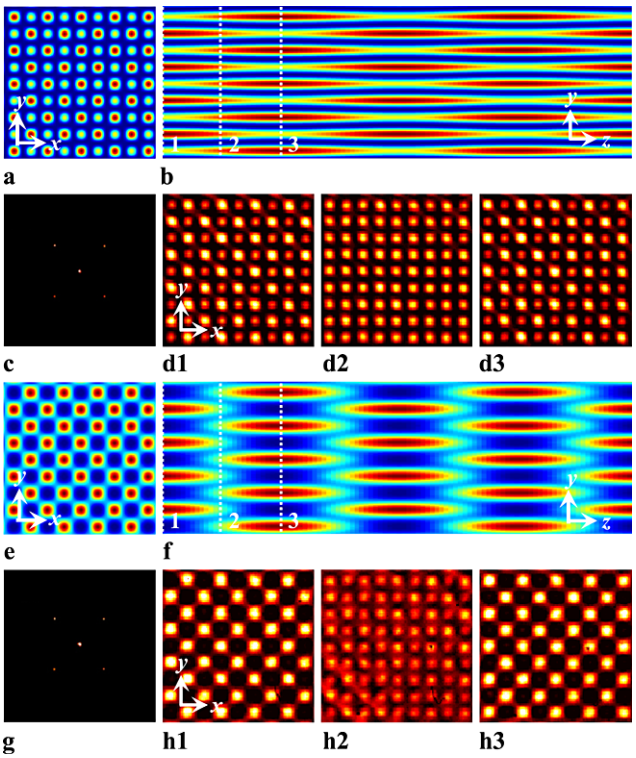

Fig. 5 Numerical (**a**, **b**, **e**–**f**) and experimental (**c**, **d**, **g**, **h**) demonstration of optical induction method for generation of 3D photonic lattices with controlled Talbot effect. (**a**, **e**) Transverse intensity patterns of lattice-inducing beam at input; (**b**, **f**) side views of grid-like patterns in (**a**, **e**) propagating along longitudinal z-direction; (**c**, **g**) spectra of the lattice-inducing beam; (**d**, **h**) transverse intensity patterns of lattice-inducing beam at different propagation distances marked by *dashed lines* in (**b**, **f**). *Top two panels* correspond to square lattices with low modulation depth, while *bottom two panels* correspond to 'ionic-type' lattices with high modulation depth

with out-of-phase modulation along the z-direction. Therefore, by adjusting the relative intensity between the 0th order ($|A_0|^2$) and the 1st order ($|A_1|^2$), which can be done by fine filtering at the Fourier plane of the amplitude masks, we can obtain 3D photonic lattices with different z-modulations. Figure 5 shows typical examples of our numerical simulation and experimental results. As shown in our previous work [16, 17, 39–41], when the 0th order is totally blocked, perfect 2D photonic lattices are created. When we gradually increase the intensity ratio between the 0th-order and the 1st-order diffracted beams at the Fourier plane, the out-of-phase index modulation along the z-direction appears and increases gradually, as depicted in Figs. 5a–5d. With a further increase of the intensity ratio to a certain value, the square lattice turns into a 'chess-board' lattice, and a complete out-of-phase modulation is achieved (meaning the intensity in a lattice site can change from bright to dark completely). In fact, the lattice induced in this latter case represents a typical 3D ionic-type photonic lattice (Figs. 5e–5h), which could be used for unusual beam control such as sup-

pression of Bragg reflection [49, 50]. Our experimental results agree well with those obtained from numerical simulations.

Further numerical simulations indicate that beam propagation in optically induced 3D ionic-type photonic lattices exhibits a variety of intriguing properties in comparison with previously studied 3D lattices due to the coexistence of the positive and negative index potentials, including self-imaging, phase conjugation, as well as anomalous diffraction and refraction. With the 3D ionic-type photonic lattices (which can be made with several modulation periods along the z-direction even within a 10-mm-long crystal), we are actively improving our linear image transmission results based on CDT [35], as an alternative yet effective image transmission scheme compared to those based on nonlinear arbitrarily shaped gap solitons [51]. Detailed theoretical and experimental studies are currently being undertaken and will be reported elsewhere.

5 Summary

We have successfully generated 3D photonic lattices in a bulk nonlinear crystal by employing different optical induction techniques, including superposition of a pair of 2D photonic lattices and reconfiguration of z-modulated 2D lattices with controlled Talbot effect. By fine tuning the lattice parameters such as lattice modulation and spacing, we have demonstrated some unusual behaviors of beam dynamics in such reconfigurable 3D photonic lattices, including enhanced discrete diffraction, CDT, anomalous diffraction, negative refraction, as well as CDT-based image transmission. Due to the additional periodic modulation along the propagation z-direction, these induced 3D photonic lattices provide a new opportunity for experimental exploration of discretizing light behavior and band gap control in three dimensions. It might be possible to realize a new type of all-optical beam steering and orientation-selective nonlinear self-trapping in 3D lattices. In addition, the study of wave dynamics in 3D photonic lattices may prove to be relevant to similar phenomena in other 3D discrete systems including solid-state physics and Bose-Einstein condensates (BECs) trapped in 3D optical lattices.

Acknowledgements This work was supported by NSF, AFOSR, and the 973 program (2007CB613203). We thank Y. Hu, R. Egger, S. Liu, C. Lou, A. Szameit, and Y. V. Kartashov for helpful discussions and assistance.

References

1. J.D. Joannopoulos, P.R. Villeneuve, S. Fan, Nature **386**, 143 (1997)
2. E. Yablonovitch, J. Opt. Soc. Am. B **10**, 283 (1993)
3. Y. Xia, B. Gates, Z.-Y. Li, Adv. Mater. **13**, 409 (2001)
4. A. Blaaderen, R. Ruel, P. Wiltzius, Nature **385**, 321 (1997)
5. S.Y. Lin, J.G. Fleming, D.L. Hetherington, B.K. Smith, R. Biswas, K.M. Ho, M.M. Sigalas, W. Zubrzycki, S.R. Kurtz, J. Bur, Nature **394**, 251 (1998)
6. M.C. Wanke, O. Lehmann, K. Muller, Q. Wen, M. Stuke, Science **275**, 1284 (1997)
7. M. Campbell, D.N. Sharp, M.T. Harrison, R.G. Denning, A.J. Turberfield, Nature **404**, 53 (2000)
8. J.-H. Jang, C.K. Ullal, M. Maldovan, T. Gorishnyy, S. Kooi, C. Koh, E.L. Thomas, Adv. Funct. Mater. **17**, 3027 (2007)
9. D.N. Christodoulides, F. Lederer, Y. Silberberg, Nature **424**, 817 (2003)
10. F. Lederer, G.I. Stegeman, D.N. Christodoulides, G. Assanto, M. Segev, Y. Silberberg, Phys. Rep. **463**, 1 (2008)
11. S. Longhi, Laser Photonics Rev. **3**, 243261 (2009)
12. A. Szameit, S. Nolte, J. Phys. B **43**, 163001 (2010)
13. N.K. Efremidis, S. Sears, D.N. Christodoulides, J.W. Fleischer, M. Segev, Phys. Rev. E **66**, 046602 (2002)
14. J.W. Fleischer, M. Segev, N.K. Efremidis, D.N. Christodoulides, Nature **422**, 147 (2003)
15. D. Neshev, E. Ostrovskaya, Y. Kivshar, W. Krolikowski, Opt. Lett. **28**, 710 (2003)
16. H. Martin, E.D. Eugenieva, Z. Chen, D.N. Christodoulides, Phys. Rev. Lett. **92**, 123902 (2004)
17. C. Lou, X. Wang, J. Xu, Z. Chen, Phys. Rev. Lett. **98**, 213903 (2007)
18. H.S. Eisenberg, Y. Silberberg, R. Morandotti, J.S. Aitchison, Phys. Rev. Lett. **85**, 1863 (2000)
19. M.J. Ablowitz, Z.H. Musslimani, Phys. Rev. Lett. **87**, 254102 (2001)
20. T. Pertschl, T. Zentgraf, U. Peschel, A. Bräuer, F. Lederer, Phys. Rev. Lett. **88**, 093901 (2002)
21. I.L. Garanovich, A.A. Sukhorukov, Y.S. Kivshar, Phys. Rev. E **74**, 066609 (2006)
22. S. Longhi, Opt. Lett. **31**, 1857 (2006)
23. S. Longhi, M. Marangoni, M. Lobino, R. Ramponi, P. Laporta, E. Cianci, V. Foglietti, Phys. Rev. Lett. **96**, 243901 (2006)
24. A. Szameit, Y.V. Kartashov, F. Dreisow, M. Heinrich, T. Pertsch, S. Nolte, A. Tünnermann, V.A. Vysloukh, F. Lederer, L. Torner, Phys. Rev. Lett. **102**, 153901 (2009)
25. Y.V. Kartashov, A. Szameit, V.A. Vysloukh, L. Torner, Opt. Lett. **34**, 2906 (2009)
26. A. Szameit, I.L. Garanovich, M. Heinrich, A.A. Sukhorukov, F. Dreisow, T. Pertsch, S. Nolte, A. Tünnermann, Y.S. Kivshar, Nat. Phys. **5**, 271 (2009)
27. K. Shandarova, C.E. Rüter, D. Kip, K.G. Makris, D.N. Christodoulides, O. Peleg, M. Segev, Phys. Rev. Lett. **102**, 123905 (2009)
28. G. Della Valle, M. Ornigotti, E. Cianci, V. Foglietti, P. Laporta, S. Longhi, Phys. Rev. Lett. **98**, 263601 (2007)
29. S. Longhi, Phys. Rev. B **77**, 195326 (2008)
30. P. Zhang, C. Lou, S. Liu, J. Zhao, J. Xu, Z. Chen, Opt. Lett. **35**, 892 (2010)
31. N.K. Efremidis, P. Zhang, Z. Chen, D.N. Christodoulides, C.E. Rüter, D. Kip, Phys. Rev. A **81**, 053817 (2010)
32. K. Staliunas, R. Herrero, Phys. Rev. E **73**, 016601 (2006)
33. H. Leblond, B.A. Malomed, D. Mihalache, Phys. Rev. E **76**, 026604 (2007)
34. P. Zhang, R. Egger, Z. Chen, Opt. Express **17**, 13151 (2009)
35. P. Zhang, N.K. Efremidis, A. Miller, Y. Hu, Z. Chen, Opt. Lett. **35**, 3252 (2010)
36. J. Xavier, P. Rose, B. Terhalle, J. Joseph, C. Denz, Opt. Lett. **34**, 2625 (2009)
37. J. Xavier, M. Boguslawski, P. Rose, J. Joseph, C. Denz, Adv. Mater. **22**, 356 (2010)

38. J. Xavier, J. Joseph, Opt. Lett. **36**, 403 (2011)
39. Z. Chen, H. Martin, E.D. Eugenieva, J. Xu, A. Bezryadina, Phys. Rev. Lett. **92**, 143902 (2004)
40. I. Makasyuk, Z. Chen, J. Yang, Phys. Rev. Lett. **96**, 223903 (2006)
41. Z. Chen, J. Yang, in *Nonlinear Optics and Applications*, ed. by H. Abdeldayem, D.O. Frazier. Research Signpost, Kerala (2007)
42. G. Bartal, O. Cohen, H. Buljan, J.W. Fleischer, O. Manela, M. Segev, Phys. Rev. Lett. **94**, 163902 (2005)
43. S. Liu, P. Zhang, X. Gan, F. Xiao, J. Zhao, Appl. Phys. B **99**, 727 (2010)
44. N.K. Efremidis, J. Hudock, D.N. Christodoulides, J.W. Fleischer, O. Cohen, M. Segev, Phys. Rev. Lett. **91**, 213906 (2003)
45. C.E. Creffield, Phys. Rev. B **67**, 165301 (2003)
46. A. Locatelli, M. Conforti, D. Modotto, C. De Angelis, Opt. Lett. **30**, 2894 (2005)
47. A. Locatelli, M. Conforti, D. Modotto, C. De Angelis, Opt. Lett. **31**, 1343 (2006)
48. C.R. Rosberg, D.N. Neshev, A.A. Sukhorukov, Y.S. Kivshar, W. Krolikowski, Opt. Lett. **30**, 2293 (2005)
49. P. Zhang, C. Lou, S. Liu, F. Xiao, J. Zhao, J. Xu, Z. Chen, Opt. Photonics News **19**, 25 (2008)
50. P. Zhang, S. Liu, C. Lou, F. Xiao, X. Wang, J. Zhao, J. Xu, Z. Chen, Phys. Rev. A **81**, 041801(R) (2010)
51. J. Yang, P. Zhang, M. Yoshihara, Y. Hu, Z. Chen, Opt. Lett. **36**, 772 (2011)